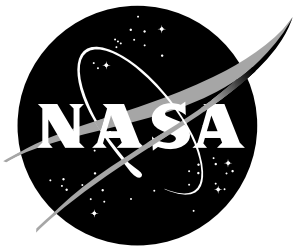
NASA/TM–20260009035



A Flight-Data Pipeline for Performance Model Identification of a Distributed Electric Propulsion Subscale Vehicle

Mia Scoblic[1], Andrew Patterson[2], Michael Acheson[2], and Venanzio Cichella[1]

[1] *University of Iowa, Iowa City, Iowa*
[2] *NASA Langley Research Center, Hampton, Virginia*

October 2026

NASA STI Program Report Series

Since its founding, NASA has been dedicated to the advancement of aeronautics and space science. The NASA scientific and technical information (STI) program plays a key part in helping NASA maintain this important role.

The NASA STI program operates under the auspices of the Agency Chief Information Officer. It collects, organizes, provides for archiving, and disseminates NASA's STI. The NASA STI program provides access to the NTRS Registered and its public interface, the NASA Technical Reports Server, thus providing one of the largest collections of aeronautical and space science STI in the world. Results are published in both non-NASA channels and by NASA in the NASA STI Report Series, which includes the following report types:

- TECHNICAL PUBLICATION. Reports of completed research or a major significant phase of research that present the results of NASA Programs and include extensive data or theoretical analysis. Includes compilations of significant scientific and technical data and information deemed to be of continuing reference value. NASA counterpart of peer-reviewed formal professional papers but has less stringent limitations on manuscript length and extent of graphic presentations.
- TECHNICAL MEMORANDUM. Scientific and technical findings that are preliminary or of specialized interest, e.g., quick release reports, working papers, and bibliographies that contain minimal annotation. Does not contain extensive analysis.
- CONTRACTOR REPORT. Scientific and technical findings by NASA-sponsored contractors and grantees.
- CONFERENCE PUBLICATION. Collected papers from scientific and technical conferences, symposia, seminars, or other meetings sponsored or co-sponsored by NASA.
- SPECIAL PUBLICATION. Scientific, technical, or historical information from NASA programs, projects, and missions, often concerned with subjects having substantial public interest.
- TECHNICAL TRANSLATION. English-language translations of foreign scientific and technical material pertinent to NASA's mission.

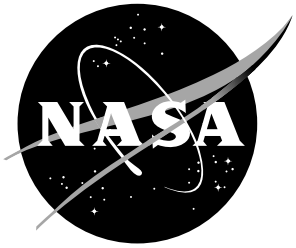
Specialized services also include organizing and publishing research results, distributing specialized research announcements and feeds, providing information desk and personal search support, and enabling data exchange services.

For more information about the NASA STI program, see the following:

- Access the NASA STI program home page at http://www.sti.nasa.gov
- Help desk contact information:

https://www.sti.nasa.gov/sti-contact-form/ and select the "General" help request type.

NASA/TM–20260009035



A Flight-Data Pipeline for Performance Model Identification of a Distributed Electric Propulsion Subscale Vehicle

Mia Scoblic[1], Andrew Patterson[2], Michael Acheson[2], and Venanzio Cichella[1]

[1] *University of Iowa, Iowa City, Iowa*
[2] *NASA Langley Research Center, Hampton, Virginia*

National Aeronautics and
Space Administration

Langley Research Center
Hampton, Virginia 23681-2199

October 2026

The use of trademarks or names of manufacturers in this report is for accurate reporting and does not constitute an official endorsement, either expressed or implied, of such products or manufacturers by the National Aeronautics and Space Administration.

Available from:

NASA STI Program / Mail Stop 148
NASA Langley Research Center
Hampton, VA 23681-2199
Fax: 757-864-6500

Abstract

Performance models are needed for trajectory optimization and guidance design but can be difficult to obtain for small research aircraft. This paper uses onboard data from six remotely piloted flights to identify a nonlinear point-mass performance model for a 9-ft-wingspan fixed-wing research aircraft. The data were synchronized, filtered, segmented by flight phase, and fitted using least squares. The identified functions map airspeed, pitch, bank angle, and motor command to vertical speed, curvature, and airspeed rate. Leave-one-flight-out cross-validation produced test R^2 values of 0.93 and 0.93 for the climb and curvature models, respectively. The identified curvature coefficient was $c_\kappa = 0.78$. The airspeed-rate model produced a test R^2 of 0.61 for the gravity-corrected response and captured the dominant longitudinal behavior. An in-sample forward simulation reproduced the measured airspeed over a representative interval without divergence. The resulting model supports preliminary three-dimensional trajectory generation within conservative, flight-supported design bounds and can be reidentified as the vehicle configuration changes.

1 Introduction

Trajectory optimization and guidance design require models that relate inputs to vehicle motion across an operating region. For fixed-wing aircraft, these models describe performance relationships such as vertical speed, curvature, and airspeed rate. This work identifies these relationships from recorded flight data for trajectory-level prediction.

Obtaining these functions can be challenging for small research aircraft. Their structures and configurations may be sensitive to small changes, and limited space constrains instrumentation. Low mass and inertia, low wing loading, and low Reynolds numbers can further complicate dynamic modeling [1]. Small excitations may be obscured by atmospheric disturbances, whereas larger excitations can drive the aircraft into nonlinear regimes. Flight-data-based identification provides a practical means of characterizing the current vehicle configuration using available onboard measurements. The objective of this work is to identify the empirical performance functions and flight-supported bounds needed for trajectory-level prediction.

Prior research demonstrates the use of scaled aircraft for flight-dynamics and control-system experiments, including the NASA AirSTAR testbed [2]. More recent work has addressed dynamic modeling for a quarter-scale distributed electric propulsion (DEP) aircraft [3]. NASA's SUbsonic Single Aft eNgine (SUSAN) Electrofan was a hybrid-electric transport concept associated with DEP research [4]. Related studies examined DEP architectures and control allocation [5–7]. Full system identification was not possible because the aircraft lacked instrumented actuators and differential-thrust allocation. This study therefore develops a baseline performance model for trajectory-level applications.

This paper develops an empirical performance model for the DEP Research Drones v1 (DEPRD v1), a 9-ft-wingspan fixed-wing unmanned aerial vehicle operated by NASA as a low-cost DEP research platform. The available sensing and actuation constrain the states, inputs, and transient behavior that can be identified from the recorded flights. DEPRD v1 uses a lightweight foam airframe that supports configuration changes and iterative flight testing. The identified relationships map measured states and commands to response variables without resolving the contributions of individual actuators. These preliminary flights did not include instrumented actuators or differential-thrust allocation.

The proposed model combines empirical performance relationships with nonlinear point-mass equations of motion. The climb relationship maps airspeed and pitch to vertical speed, the curvature relationship maps airspeed and bank angle to heading rate, and the airspeed-rate relationship maps motor command, airspeed, and pitch to $\dot{V}$. Pitch, bank angle, and airspeed rate are treated as trajectory-level control inputs. A separate empirical function maps motor command to airspeed rate when a command-based representation is required. The model represents trajectory-level behavior over the conditions contained in the flight data. It does not characterize transient aircraft modes, identify individual actuator effects, or replace an aerodynamic database.

Data recorded onboard DEPRD v1 during six remotely piloted flights are used to identify the model parameters. The data are synchronized, filtered, and segmented into operational phases before the performance relationships are fitted using least squares. Leave-one-flight-out cross-validation evaluates consistency across flights, and an in-sample forward simulation evaluates airspeed propagation.

The principal contributions are a flight-data-based performance model for DEPRD v1, conservative bounds for preliminary trajectory design, and an evaluation of model consistency across six flights. The flight-supported bounds identify conditions sufficiently represented in the available data for preliminary trajectory design. They do not represent the physical limits, certified flight envelope, or complete empirical envelope of DEPRD v1.

Potential applications of this model include optimal motion-planning methods based on Bernstein approximations [8–10] and evaluation of trajectories generated by learning-based methods [11, 12]. Because the parameters are identified from onboard flight data, the procedure can be repeated as the airframe, propulsion system, or test configuration changes. Additional flights with more varied maneuvers and actuator measurements will be required to expand the supported operating region and identify a dynamic vehicle model.

The remainder of this paper is organized as follows. Section 2 presents the nonlinear point-mass model and empirical performance functions. Section 3 describes the flight-data processing, phase segmentation, parameter-identification, and cross-validation procedures. Section 4 presents the flight-supported trajectory-design bounds, identified coefficients, and model-evaluation results. Section 5 summarizes the findings and identifies directions for future work.

2 Model Formulation

The aircraft is represented by a nonlinear point-mass model in which pitch, bank angle, and airspeed rate serve as trajectory-level control inputs. Airspeed rate is treated as a virtual input rather than modeling motor command directly in the equations of motion. A separate empirical function, $f_a(V, T, \theta)$, maps motor command to airspeed rate when a command-based representation is required. This formulation separates trajectory planning from the vehicle-specific relationship between motor command and airspeed rate.

The state and trajectory-level control vectors are

$$\mathbf{x} = [x \; y \; h \; \psi \; V]^T, \qquad \mathbf{u} = [\theta \; \phi \; a]^T, \tag{1}$$

where x and y are horizontal position coordinates, h is altitude, ψ is heading, V is airspeed, θ is pitch angle, ϕ is bank angle, and $a \equiv \dot{V}$ is airspeed rate. Angles are expressed in radians when evaluating the model.

The point-mass dynamics are

$$\begin{aligned} \dot{x} &= V_h \cos\psi, \\ \dot{y} &= V_h \sin\psi, \\ \dot{h} &= f_h(V, \theta), \\ \dot{\psi} &= V_h f_\kappa(V, \phi), \\ \dot{V} &= a, \end{aligned} \tag{2}$$

where

$$V_h = \sqrt{V^2 - \dot{h}^2} \tag{3}$$

is the horizontal component of airspeed. The position equations neglect wind. If wind is included, the horizontal wind-velocity components must be added to $\dot{x}$ and $\dot{y}$.

The empirical functions use the following parameterizations. Vertical speed is modeled as a linear function of airspeed and pitch:

$$f_h(V, \theta) = b_0 + b_1 V + b_2 \theta, \tag{4}$$

where b_0, b_1, and b_2 are identified coefficients.

Planar curvature is modeled as

$$f_\kappa(V, \phi) = c_\kappa \frac{g}{V^2} \tan\phi, \tag{5}$$

where g is gravitational acceleration and c_κ is an empirical scaling coefficient. This planar approximation neglects three-dimensional kinematic effects, taking $V_h = V\cos\gamma \approx V$ for small flight-path angles, $|\gamma| \ll 1$.

Airspeed rate may be specified directly through the virtual input a. When a command-based representation is needed, a is replaced by

$$a = f_a(V, T, \theta) = c_0 + c_1 T + c_2 T^2 + c_3 T^3 - k_D V^2 - g\sin\theta, \tag{6}$$

where $T \in [0, 1]$ is the throttle command, c_0 through c_3 define its empirical contribution, and k_D is an effective quadratic airspeed coefficient. In this form, the control vector is $[\theta\ \phi\ T]^T$, and airspeed rate is determined by Eq. 6.

The identified parameter vector is

$$\boldsymbol{\eta} = [b_0,\ b_1,\ b_2,\ c_\kappa,\ c_0,\ c_1,\ c_2,\ c_3,\ k_D]^T. \tag{7}$$

Trajectory generation is restricted using conservative bounds supported by the analyzed flight data:

$$V_{\min} \le V \le V_{\max}, \qquad \dot{h}_{\min} \le \dot{h} \le \dot{h}_{\max}, \qquad |\kappa| \le \kappa_{\max} = \frac{1}{R_{\min}}. \tag{8}$$

3 Methods

Flight data were collected from a 9-ft-wingspan foam aircraft equipped with a Pixhawk Cube Orange flight controller running PX4 autopilot software. Data from six remotely piloted flights were recorded using PX4's ULog system and extracted using the `pyulog` library.

The recorded data streams had different sampling frequencies: vehicle angular velocity was recorded at 50 Hz, attitude and acceleration at 20 Hz, local position estimates at 10 Hz, and airspeed at 5 Hz. The local-position timestamps were used as the common time vector. All other continuous signals were linearly interpolated onto this vector, resulting in a nominal sampling rate of 10 Hz. A third-order Savitzky–Golay smoother with a 51-sample window was applied to airspeed, vertical speed, pitch, and bank angle. Airspeed rate was obtained by applying the corresponding first-derivative Savitzky–Golay smoother to the interpolated airspeed signal. Heading derived from the attitude quaternion was unwrapped and differentiated to obtain heading rate. The processed signals were used for flight-phase segmentation, model identification, and evaluation.

A rule-based segmentation algorithm separated each flight into takeoff (TO), landing (LND), and three airborne maneuver categories: straight and level (S&L), ascent/descent (A/D), and turn (TURN). Altitude was referenced to the first local-position sample in each flight log. The landed state was obtained from the PX4 `vehicle_land_detected` topic. The algorithm calculated the median altitude among samples above 5 m and defined the transition altitude as 5 m below that value. Samples between liftoff and the first crossing of the transition altitude were classified as takeoff. Samples after the final crossing of that altitude and before landing were classified as landing. Samples above the transition altitude were classified according to bank angle and vertical speed:

- **TURN:** bank-angle magnitude greater than 8.0°;
- **S&L:** bank-angle magnitude of 8.0° or less and vertical speed within ±0.5 m/s; and
- **A/D:** bank-angle magnitude of 8.0° or less and vertical speed outside ±0.5 m/s.

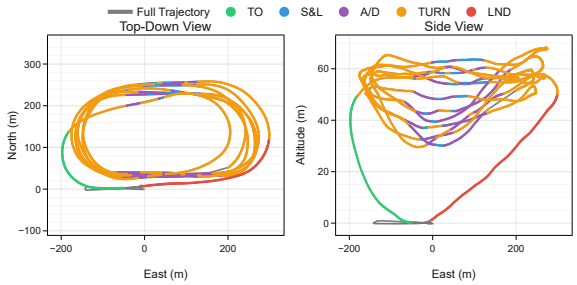


Figure 1: Three-dimensional flight path color-coded by operational phase: takeoff, straight-and-level, ascent/descent, turn, and landing.

Figure 1 shows a representative flight path color-coded by operational phase. The classifications were checked against altitude, bank angle, vertical speed, and temporal progression to confirm separation of the five phases.

Figure 2 shows the altitude and bank-angle histories for a representative flight. The altitude criterion isolates takeoff and landing, and the bank-angle threshold identifies turning segments. The remaining airborne samples are separated into straight-and-level and ascent/descent segments according to vertical speed.

The climb and airspeed-rate models were identified using an in-air dataset defined independently of the maneuver classifications. A sample was included when the aircraft was not classified as landed, airspeed exceeded 5 m/s, and altitude exceeded 2 m above the local reference. The climb model in Eq. 4 used vertical speed as the response and airspeed and pitch as predictors. The airspeed-rate model in Eq. 6 used differentiated airspeed as the response and motor command, airspeed, and pitch as predictors.

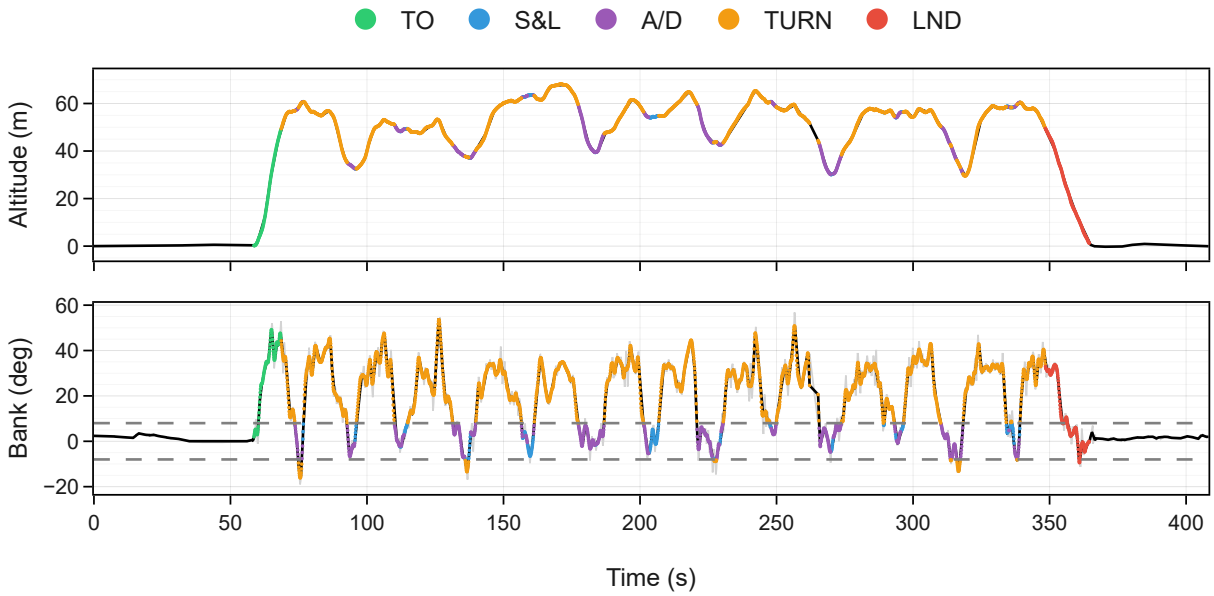


Figure 2: Altitude and bank-angle time histories color-coded by operational phase for a representative flight.

A separate steady-turn dataset was defined to identify the curvature coefficient in Eq. 5. The dataset was intended to exclude brief roll transients and other nonsteady maneuvers. Samples were required to satisfy the in-air criterion, have a bank-angle magnitude of at least 5.0°, have a heading-rate magnitude of at least 5.0°/s, have a pitch-angle magnitude below 5.0°, and have an airspeed-rate magnitude below 0.5 m/s^2.

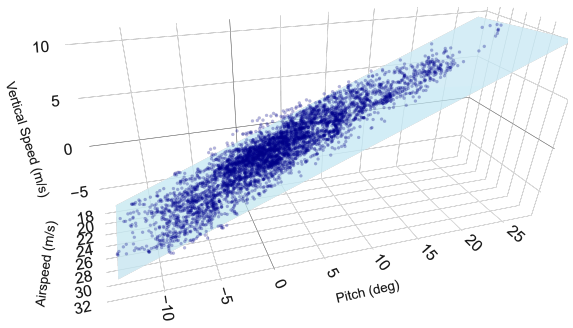


Figure 3: Fitted climb surface overlaid on measured flight data, mapping vertical speed as a function of airspeed and pitch.

All coefficients were identified using least squares. For the climb model, vertical speed was regressed against the constant, airspeed, and pitch terms in Eq. 4. Figure 3 shows the fitted climb surface overlaid on the measured data.

For the airspeed-rate model, the known gravitational term was moved to the response side of Eq. 6, such that $a + g\sin\theta$ was used as the regression target. This response was regressed against a constant, the linear, quadratic, and cubic motor-command terms, and the negative squared-airspeed term. The fitted function $f_a(V, T, \theta)$ maps motor command, airspeed, and pitch to airspeed rate.

For the curvature model, heading was unwrapped and differentiated to obtain the measured heading rate, $\dot{\psi}$. Measured heading rate was regressed against the kinematic prediction from Eqs. 2 and 5. The regression was constrained to pass through the origin, and its slope provided c_κ. Figure 4 shows the resulting fit.

Conservative trajectory-design bounds were derived from the pooled data from all six flights. Airspeed bounds were defined by the 2nd and 98th percentiles, and vertical-speed bounds were defined by the 5th and 95th percentiles. Nominal airspeed was defined as the median airspeed among straight-and-level samples. The bank-angle value used to calculate the curvature bound was the 95th percentile of the bank-angle magnitude in the steady-turn dataset. The minimum design turn radius and maximum design curvature were then derived from the nominal airspeed, bank-angle percentile, and identified curvature coefficient using Eqs. 5 and 8.

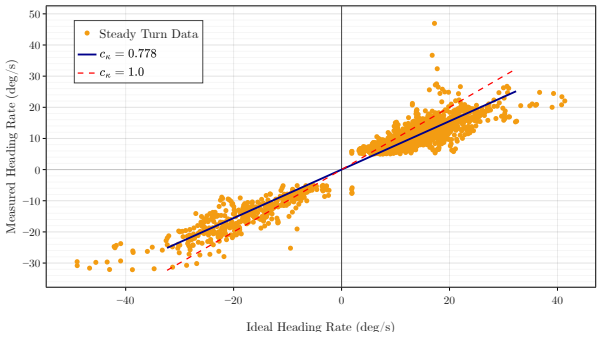


Figure 4: Measured heading rate versus the kinematic heading-rate prediction for the steady-turn dataset. The fitted slope is c_κ.

Model consistency across flights was evaluated using leave-one-flight-out cross-validation. For each fold, a model was fitted using five flights and evaluated on the remaining flight. Predictions from all six held-out flights were pooled before the test R^2 and RMSE were calculated. Full-data metrics were calculated from the model fitted to the pooled data from all six flights. For the airspeed-rate model, the reported metrics were calculated for the gravity-corrected response $a + g\sin\theta$. The identified coefficients and evaluation metrics are summarized in Table 2.

Forward simulation was used to evaluate the airspeed-rate model separately from its instantaneous regression fit. The simulation was initialized with measured airspeed and propagated using explicit Euler integration of the airspeed rate predicted by $f_a(V, T, \theta)$ at the recorded time intervals. At each subsequent time step, the propagated airspeed was supplied to the model in place of measured airspeed. The recorded motor-command and pitch histories were retained as inputs. Because the displayed flight was included in the full-data identification set, this simulation is an in-sample evaluation rather than independent validation.

4 Results

Table 1 summarizes the flight-supported design values derived from the six analyzed flights.

Table 1: Flight-supported design values derived from the six analyzed flights.

	V (m/s)	V_{nom} (m/s)	$\dot{h}$ (m/s)	ϕ_{95} (°)	R_{min} (m)	κ_{max} (m^{-1})
Bounds	[20.0, 29.2]	24.4	[−4.35, 4.87]	49.2	66	0.0152

Figure 5 shows the distributions of measured and derived flight variables across the segmented phases. Elevated heading rates and bank-angle magnitudes align with the TURN classification. The A/D phase spans positive and negative vertical speeds, corresponding to ascent and descent, while takeoff is associated primarily with positive vertical speed. These distributions show the conditions represented in the identification data.

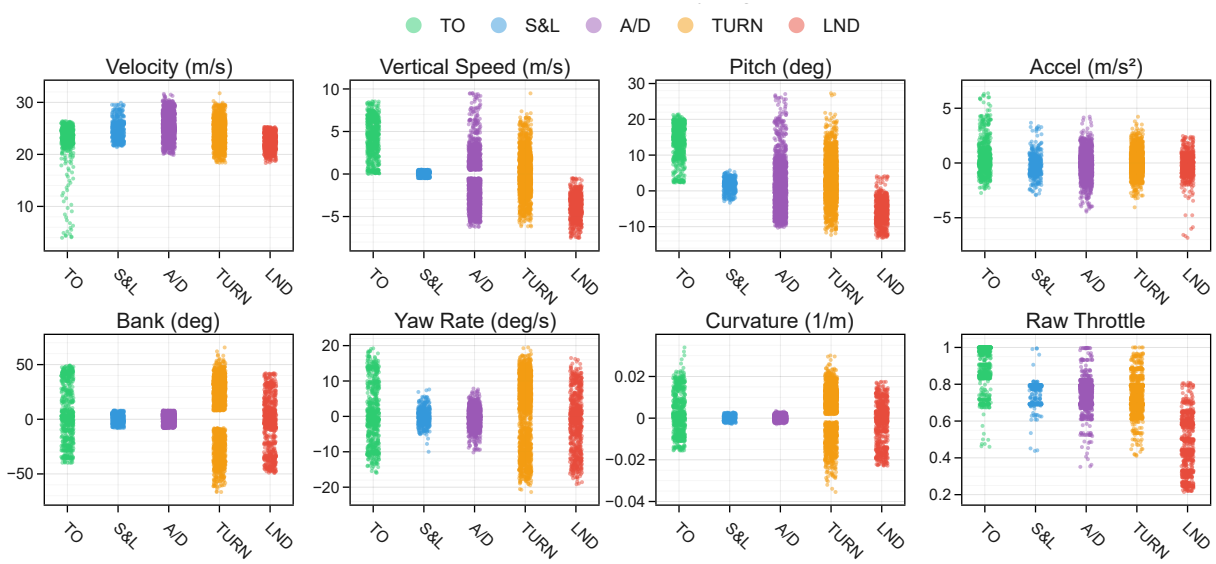


Figure 5: Distributions of flight variables across the five operational phases for the six analyzed flights.

The bounds and distributions are derived from six flights covering similar operating conditions. Although these data support preliminary modeling within the observed conditions, broader trajectory design will require additional flights with deliberately varied maneuvers.

Table 2 presents the identified climb, curvature, and airspeed-rate parameters and their leave-one-flight-out cross-validation metrics. The climb coefficients use airspeed and vertical speed in meters per second and pitch in radians. The curvature RMSE is calculated for heading rate, and the airspeed-rate metrics are calculated for the gravity-corrected response $a + g \sin\theta$.

The climb and curvature models achieved test R^2 values of 0.93 and 0.93, respectively. The differences between the full-data and test values were 0.002 for the climb model and less than 0.001 for the curvature model. These results indicate consistent performance across the six held-out flights.

The curvature coefficient was identified as $c_\kappa = 0.78$. Over the analyzed steady-turn conditions, the measured heading rate was approximately 78% of the kinematic prediction. The remaining variation is not represented by the constant curvature coefficient.

The airspeed-rate model produced a test R^2 of 0.610 for the gravity-corrected response. Airspeed rate was obtained by differentiating airspeed and was therefore sensitive to measurement noise and numerical-differentiation error. Wind variation, propulsion-response dynamics, and battery-voltage variation may also contribute behavior not represented by the static function $f_a(V, T, \theta)$. Nevertheless, the model captured the dominant relationship among motor command, airspeed, pitch, and airspeed rate.

Table 2: Identified model parameters and leave-one-flight-out cross-validation results.

Model	Identified parameters	Evaluation results
Climb Eq. 4	$b_0 = -3.106$, $b_1 = 0.0829$, $b_2 = 23.377$	**Full-data** R^2**:** 0.929 **Test** R^2**:** 0.927 **Test RMSE:** 0.738 m/s
Curvature Eq. 5	$c_\kappa = 0.778$	**Full-data** R^2**:** 0.932 **Test** R^2**:** 0.932 **Test RMSE:** 0.0581 rad/s
Airspeed rate Eq. 6	$c_0 = -0.822$, $c_1 = 6.837$, $c_2 = -2.795$ $c_3 = 3.217$, $k_D = 0.00598$	**Full-data** R^2**:** 0.673 **Test** R^2**:** 0.610 **Test RMSE:** 0.681 m/s^2

Figure 6 provides an in-sample evaluation of the airspeed-rate model using a representative flight. The top panel compares measured airspeed rate with the instantaneous prediction from $f_a(V, T, \theta)$ using measured airspeed, motor command, and pitch. The bottom panel shows a forward simulation initialized from measured airspeed and propagated by integrating the predicted airspeed rate. At each subsequent time step, the simulated airspeed was supplied to $f_a(V, T, \theta)$ while the recorded motor-command and pitch histories were retained as inputs. The full-data model reproduced the measured airspeed over the selected interval without divergence. Because the evaluated flight was included in the identification dataset, this result demonstrates in-sample consistency rather than independent predictive performance.

5 Conclusions

This work identified a nonlinear point-mass performance model for a subscale fixed-wing research aircraft using onboard data from six remotely piloted flights. The available flight logs supported identification of the vertical-speed, curvature, and airspeed-rate relationships required by the selected model.

The climb and curvature models performed consistently across the six held-out flights. The identified curvature coefficient, $c_\kappa = 0.7777$, indicates that the measured heading rate was approximately 78% of the kinematic prediction over the analyzed steady-turn conditions.

The airspeed-rate model had greater prediction error because it relies on differentiated airspeed and does not represent wind variation, propulsion transients, or battery-voltage variation. Nevertheless, it captured the dominant response to motor command, airspeed, and pitch. The full-data model also reproduced measured airspeed over a representative in-sample interval without divergence.

The resulting parameter set supports preliminary trajectory optimization and guidance design within the flight-supported bounds established in this study. Broader application will require flights with more varied maneuvers, instrumented actuator and propulsion measurements, and independent evaluation of generated three-dimensional trajectories.

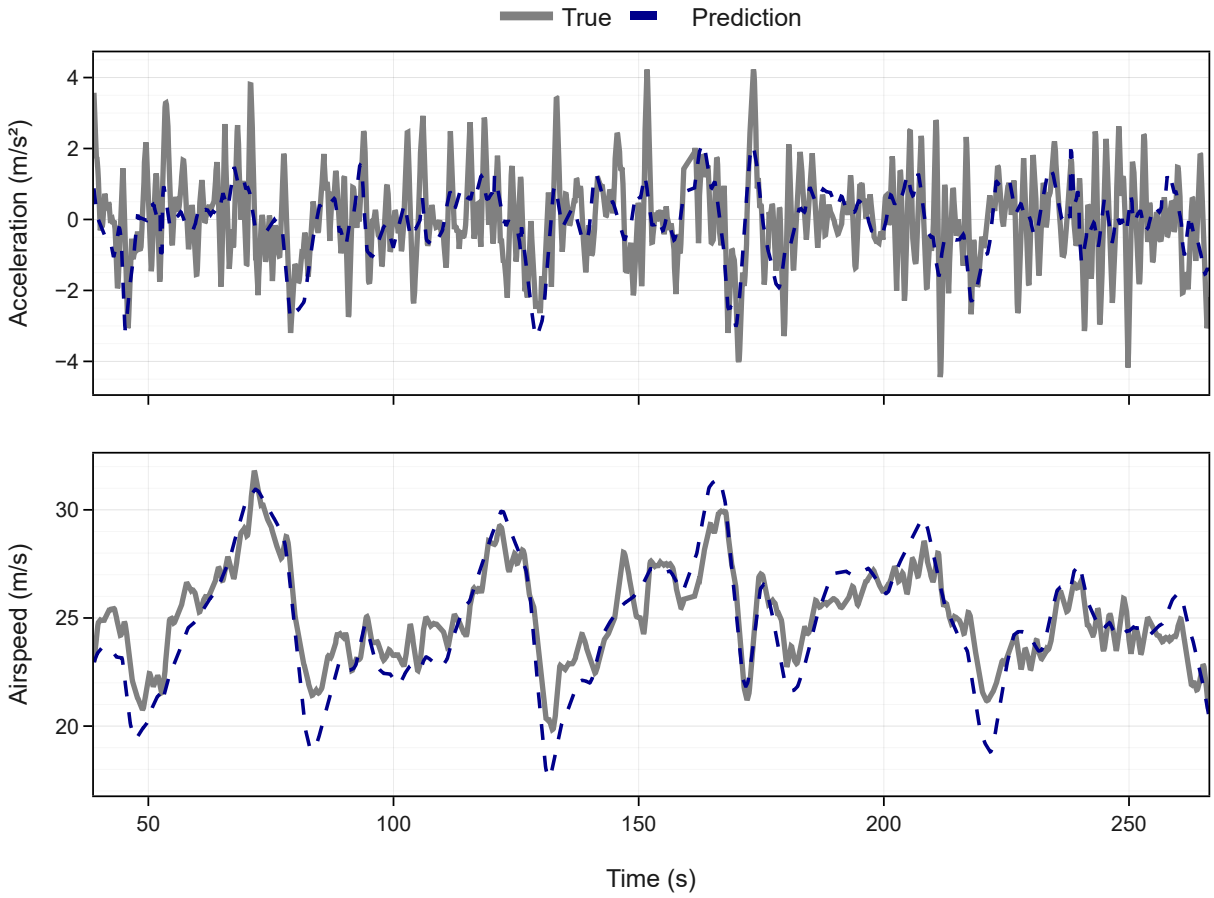


Figure 6: Instantaneous airspeed-rate prediction (top) and forward-simulated airspeed (bottom) compared with recorded data over a representative in-sample flight interval.

Acknowledgments

This work was supported by NASA Grant 80NSSC23M0117 and the TTT-APA subproject. The authors gratefully acknowledge Jonathan Litt and Ralph Jansen for technical guidance and manuscript review, and Robert McSwain, Brian Duvall, and Brayden Chamberlain for their support of the flight test activities.

References

1. Simmons, B. M., McClelland, H. G., and Woolsey, C. A., "Nonlinear model identification methodology for small, fixed-wing, unmanned aircraft," *Journal of Aircraft*, Vol. 56, No. 3, 2019, pp. 1056–1067.

2. Jordan, T., and Bailey, R., "Nasa langley's airstar testbed: a subscale flight test capability for flight dynamics and control system experiments," *AIAA guidance, navigation and control conference and exhibit*, 2008, p. 6660.

3. Litt, J. S., Hernandez, E. E., Liu, S. J., Steiner, J. P., Sowers, T. S., Owen, A. K., Sachs-Wetstone, J. J., Dever, T. P., Stalcup, E. J., Hill, E. D., et al., "Preliminary Dynamic Modeling of a Quarter-Scale Distributed Electric Propulsion Aircraft," *AIAA AVIATION 2026 Forum*, 2026, p. 4786.

4. Jansen, R. H., French, B. D., Glaser, L., Dever, T. P., Stalcup, E. J., Litt, J. S., Ellafrits, S. A., Kowalewski, S. R., Chau, T., Machado, L. M., et al., *Subsonic Single Aft Engine (SUSAN) Electrofan Project*, National Aeronautics and Space Administration, Glenn Research Center, 2025.

5. Ogden, N. C., and Patterson, A., "A Framework for Evaluating Distributed Electric Propulsion on the SUSAN Electrofan Aircraft," Tech. rep., 2023.

6. Litt, J. S., "Optimal Control Allocation for Distributed Electric Propulsion in a Series/Parallel Partial Hybrid Powertrain," *Journal of Engineering for Gas Turbines and Power*, Vol. 147, No. 1, 2025, p. 011028.

7. Litt, J. S., "Power Optimal Control Allocation for Distributed Electric Propulsion in a Series Hybrid Powertrain," *AIAA AVIATION 2026 Forum*, 2026, p. 4687.

8. Cichella, V., Kaminer, I., Walton, C., and Hovakimyan, N., "Optimal motion planning for differentially flat systems using Bernstein approximation," *IEEE Control Systems Letters*, Vol. 2, No. 1, 2017, pp. 181–186.

9. Patterson, A., MacLin, G., Acheson, M., Tabasso, C., Cichella, V., and Gregory, I., "On Hermite interpolation using Bernstein polynomials for trajectory generation," 2023.

10. MacLin, G., Cichella, V., Patterson, A., Acheson, M., and Gregory, I., "Optimal control using composite Bernstein approximants," *2024 IEEE 63rd Conference on Decision and Control (CDC)*, IEEE, 2024, pp. 8276–8281.

11. MacLin, G., Cichella, V., Patterson, A., and Gregory, I., "Real-time optimal control via transformer networks and Bernstein polynomials," *2025 IEEE 64th Conference on Decision and Control (CDC)*, IEEE, 2025, pp. 7313–7318.

12. MacLin, G., Cichella, V., Patterson, A., and Gregory, I. M., "Transformer-enabled leg-based trajectory generation for autonomous aircraft near airports," *AIAA AVIATION FORUM AND ASCEND 2025*, 2025, p. 3269.

REPORT DOCUMENTATION PAGE

Form Approved
OMB No. 0704–0188

The public reporting burden for this collection of information is estimated to average 1 hour per response, including the time for reviewing instructions, searching existing data sources, gathering and maintaining the data needed, and completing and reviewing the collection of information. Send comments regarding this burden estimate or any other aspect of this collection of information, including suggestions for reducing this burden, to Department of Defense, Washington Headquarters Services, Directorate for Information Operations and Reports (0704-0188), 1215 Jefferson Davis Highway, Suite 1204, Arlington, VA 22202-4302. Respondents should be aware that notwithstanding any other provision of law, no person shall be subject to any penalty for failing to comply with a collection of information if it does not display a currently valid OMB control number.
PLEASE DO NOT RETURN YOUR FORM TO THE ABOVE ADDRESS.

1. REPORT DATE *(DD-MM-YYYY)*	2. REPORT TYPE	3. DATES COVERED *(From - To)*
01-10-2026	Technical Memorandum	

4. TITLE AND SUBTITLE
A Flight-Data Pipeline for Performance Model Identification of a Distributed Electric Propulsion Subscale Vehicle

5a. CONTRACT NUMBER

5b. GRANT NUMBER

5c. PROGRAM ELEMENT NUMBER

6. AUTHOR(S)
Mia Scoblic
Andrew Patterson
Michael Acheson
Venanzio Cichella

5d. PROJECT NUMBER

5e. TASK NUMBER

5f. WORK UNIT NUMBER
D316

7. PERFORMING ORGANIZATION NAME(S) AND ADDRESS(ES)
NASA Langley Research Center
Hampton, Virginia 23681-2199

8. PERFORMING ORGANIZATION REPORT NUMBER

9. SPONSORING/MONITORING AGENCY NAME(S) AND ADDRESS(ES)
National Aeronautics and Space Administration
Washington, DC 20546-0001

10. SPONSOR/MONITOR'S ACRONYM(S)
NASA

11. SPONSOR/MONITOR'S REPORT NUMBER(S)
NASA/TM–20260009035

12. DISTRIBUTION/AVAILABILITY STATEMENT
Unclassified-Unlimited
Subject Category
Availability: NASA STI Program (757) 864-9658

13. SUPPLEMENTARY NOTES

14. ABSTRACT

Performance models are needed for trajectory optimization and guidance design but can be difficult to obtain for small research aircraft. This paper uses onboard data from six remotely piloted flights to identify a nonlinear point-mass performance model for a 9-ft-wingspan fixed-wing research aircraft. The data were synchronized, filtered, segmented by flight phase, and fitted using least squares. The identified functions map airspeed, pitch, bank angle, and motor command to vertical speed, curvature, and airspeed rate. Leave-one-flight-out cross-validation produced test R^2 values of 0.93 and 0.93 for the climb and curvature models, respectively. The identified curvature coefficient was $c_\kappa = 0.78$. The airspeed-rate model produced a test R^2 of 0.61 for the gravity-corrected response and captured the dominant longitudinal behavior. An in-sample forward simulation reproduced the measured airspeed over a representative interval without divergence. The resulting model supports preliminary three-dimensional trajectory generation within conservative, flight-supported design bounds and can be reidentified as the vehicle configuration changes.

15. SUBJECT TERMS
System Identification, Equation of Motion, Flight Telemetry, Distributed Electric Propulsion

16. SECURITY CLASSIFICATION OF:			17. LIMITATION OF ABSTRACT	18. NUMBER OF PAGES	19a. NAME OF RESPONSIBLE PERSON
a. REPORT	b. ABSTRACT	c. THIS PAGE			HQ-STI-infodesk@mail.nasa.gov
U	U	U	UU	00	19b. TELEPHONE NUMBER *(Include area code)* (757) 864-9658